Journal of ELECTRONIC MATERIALS, Vol. 45, No. 10, 2016
DOI: 10.1007/s11664-016-4698-8
© 2016 The Minerals, Metals & Materials Society

Effects of Implantation Sequence on the Micro-defects in H and O Implanted Silicon

ZHUO WANG,[1,4] LIN YANG,[2] LI-ZHU ZHANG,[1] SHAO-BO SHI,[1] PENG ZHANG,[3] XING-ZHONG CAO,[3] and BAO-YI WANG[3]

1.—School of Science, Tianjin University of Technology and Education, Tianjin 300222, China. 2.—School of Physical Education, Shijiazhuang University, Shijiazhuang 050035, China. 3.—Key Laboratory of Nuclear Radiation and Nuclear Energy Technology, Institute of High Energy Physics, Chinese Academy of Sciences, Beijing 100049, China. 4.—e-mail: Wangzhuo@tute.edu.cn

Cz *n*-type Si (100) wafers are implanted with 190 keV O and 40 keV H ions in different implantation sequences. Cross sectional transmission electron microscopy and slow positron annihilation spectroscopy are used to study the formation and evolution of micro-defects. Our results clearly show that the defect morphology depends strongly on the implantation sequence. Large cavities are observed in O preimplanted samples, while only platelets are observed in H preimplanted samples. The change regularity of the *S* parameter is the same for the Si samples co-implanted at different sequences. But in H preimplanted samples, the *S* parameter is a little higher. The effects of the implantation sequence on the micro-defects have been discussed in combination with H and O implantation-induced defects as well as their interactions upon annealing.

Key words: Platelet, cavity, H implantation, silicon

INTRODUCTION

Silicon implanted with H ions suffers from various damage, such as platelets, cavities, surface blistering, and even layer splitting.[1–3] However, by virtual of this damages a technology named "Smart-Cut" has been developed to produce high quality silicon-on-insulator (SOI) wafers.[1] In addition, this technology opens up wide applications in the fabrication of material combinations. Single-crystalline SiC on glass, InP on Si, and GaAs on Si have been realized by the standard Smart-cut processes.[4–6]

It is reported that He and H co-implantation can reduce the total dose necessary to obtain layer transfers as compared to H single implantation.[7] As discussed in our previous paper, O and H sequential implantation could also promote surface damage formation.[8] For instance, the average size of craters from localized exfoliations is increased, and the thermal budget for surface blistering is reduced. These effects can not only reduce the production cost of Smart-Cut technology, but also benefit thermal mismatch between dissimilar materials during annealing for layer splitting. However, the defect microstructures induced by co-implantation of different ions rely on the details of implantation, such as sequence, temperature, and dose ratio. Therefore, more experiments are needed to better understand the defect formation in H and O co-implanted Si. In this work, H and O ions are implanted into Si with fixed doses and energies. By using cross sectional transmission electron microscopy (XTEM) and slow positron annihilation spectroscopy (SPAS), we have studied the relation between defect morphology and implantation sequences.

EXPERIMENTAL PROCEDURES

The investigated samples were prepared on *n*-type Si(100) substrates with a resistivity of 1 Ω cm–10 Ω cm. Then 190 keV O^+ and 40 keV H^+ were implanted at room temperature in different sequences. During implantation, the doses for O and H ions were $1 \times 10^{16}\ cm^{-2}$ and

(Received June 14, 2015; accepted May 24, 2016; published online June 9, 2016)

3.5×10^{16} cm^{-2}. According to the stopping and range of ions in matter (SRIM) calculations,[9] the projected range and range straggle are 381 nm and 64 nm for 40 keV H ions, respectively, and that of 190 keV O ions are 418 nm and 98 nm. After implantation, the Si wafers were cut into small pieces and then annealed in different temperatures for 1 h in the flowing ambient of N_2 gas.

XTEM observations were performed to identify the distribution and location of extended defects, platelets and cavities. XTEM samples (annealed at 800°C for an hour) were prepared in the conventional way by mechanical thinning and Ar^+ etching. The XTEM images were recorded on a Tecnai G2 F20 S-Twin microscope with an acceleration voltage of 200 kV.

Moreover, SPAS was used to study the thermal evolution of vacancy-type defects, corresponding to as-implanted, 300°C, and 400°C annealing samples. The slow positrons were implanted with energies tunable from 0.18 keV to 20 keV. The Doppler broadening of the 511 keV annihilation γ rays was recorded at room temperature. The level of the Doppler broadening is indicated by the usual S parameter, which is defined as the ratio of the counts in a fixed central region ($510.2 < E_\gamma < 511.8$ keV) of the 511 keV line to the total counts of the peak ($504.2 < E_\gamma < 517.8$ keV). The S parameter is always larger for positrons annihilated in vacancy-type defects than for positrons annihilated in the ordered bulk.

RESULTS AND DISCUSSION

XTEM investigations have been performed to observe the defect microstructures of Si co-implanted with H and O ions at different implantation sequences. After 800°C annealing, a damage band is created in O preimplanted samples at a depth of about 530 nm, as shown in Fig. 1a. It clearly shows that the damage band mainly contain cavities and dislocations, surrounded by a large strain field. From Fig. 1b and c, the cavities in the defect band can be divided into three types, according to their size and shape. Small cavities with a diameter of several nanometers are circular. Some of the large cavities with a size of 20 nm–50 nm are not circular but have some facets. The inset image in Fig. 1b gives the morphology of such a cavity, which is 39 nm and has 12 facets. However, the larger cavities in the range of 70 nm–110 nm are approximately elliptic, stretching along the defect band. As it is shown in the XTEM micrographs, large cavities are usually distributed in the middle of the defect band, surrounded by the rather small cavities.

However, the morphology of defect microstructures is quite different if changing the implantation sequence of H and O ions. After annealing at 800°C for 1 h, the micro-defects in H preimplanted samples are shown in Fig. 2. The defect band has a width of about 300 nm and is centered at a depth of

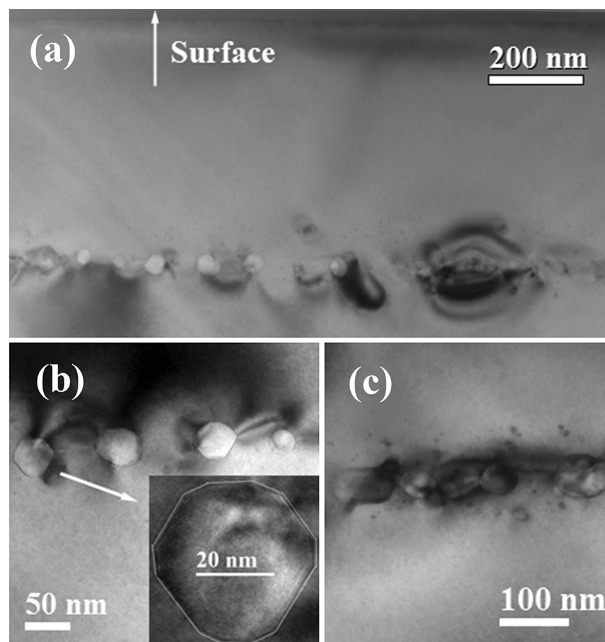

Fig. 1. XTEM micrographs showing defects created in Si sequentially implanted with 190 keV O and 40 keV H ions and followed by 800°C annealing for 1 h, (a) the overall defect morphology, (b) and (c) different areas in the defect band. The inset image gives the close view of a cavity and white lines are drawn parallel to the facets to show them clearly.

550 nm (see Fig. 2a). From the zoom-in image on the band, it is obvious there are a large number of platelets but no cavities can be found (see Fig. 2b and c). Most of the platelets are on (100) planes, which are parallel to the surface. The density of (111) platelets as pointed out by a white arrow is clearly much lower. In addition, the morphology of a platelet with the size of 12 nm is shown in the inset image of Fig. 2b.

From the XTEM results, it can be concluded that the defect morphology strongly depends on the implantation sequence of H and O ions. When two or more kinds of ions are implanted, the implantation sequence is very important and must be given full consideration. In our case, cavities (platelets) dominate the defect band in the O–(H–) preimplanted samples. The sequence effect results from H and O interacting differently with Si when being implanted and after subsequent annealing.

H implantation can introduce H atoms as well as vacancy-type defects. Since H is chemically active, a large part of H implants can react with Si atoms, dangling bonds or defects during implantation. Some of the Si–Si bonds are replaced by weaker Si–H–H–Si bonds[10] that are easily broken and form platelets after annealing. Moreover, a variety of H-vacancy complexes form around the projected range. These H-related complexes are essential for the nucleation of platelets and H_2 bubbles.[11] Several groups have studied the formation and thermal evolution of H-related complexes by infrared

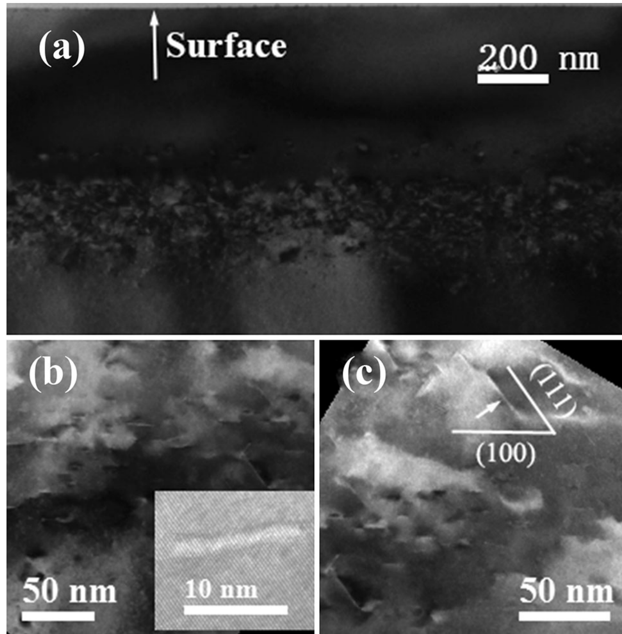

Fig. 2. XTEM micrographs showing defects created in Si sequentially implanted with 40 keV H and 190 keV O ions and followed by 800°C annealing for 1 h, (a) the overall defect morphology, (b) and (c) different areas in the defect band. Platelets on (100), which is parallel to the surface, and on (111) planes can clearly be seen. The inset image gives the close view of a platelet.

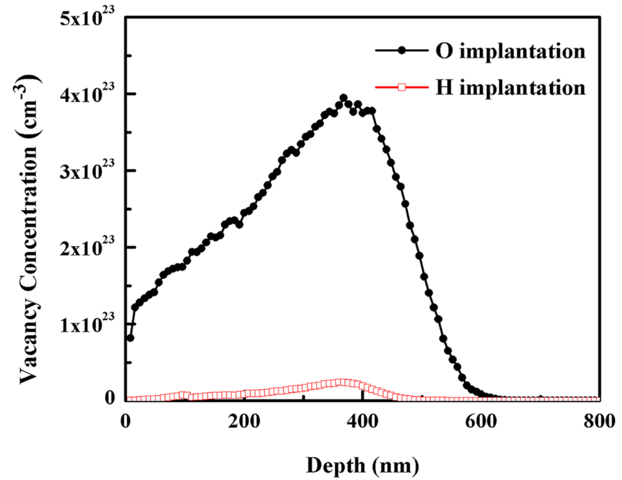

Fig. 3. SRIM simulation results showing the vacancy profiles in Si implanted by 190 keV O ions at a fluence of 1×10^{16} cm^{-2} and 40 keV H ions at a fluence of 3.5×10^{16} cm^{-2}.

absorption and Raman scattering measurements.[12–14] During annealing, H atoms are released from H-related defects and combine with each other to form H_2. After annealing at a higher temperature, H_2 molecules are movable and tend to accumulate in the platelets or H_2 bubbles rather than in interstitial places to lower the free energy of the system. The platelets and bubbles become larger and larger under the increasing internal pressure. If the pressure is high enough, these defects will connect with each other and eventually lead to surface blistering and even exfoliation.

O implantation, on the other hand, can introduce a large amount of vacancies more efficiently. Based on SRIM simulations, the vacancy concentration profiles in Si implanted with O and H ions are shown in Fig. 3. We can see that the peak concentration of vacancy defects caused by O implantation is much higher than that of H implantation, although the dose of O ions is less than that of H ions. This is an important reason why we choose O ions co-implanted with H ions. O ions are also chemically active, reacting with Si atoms to form Si–O bonds. In addition, O atoms can move in the Si lattice and diffuse to cavities or platelets after annealing at a higher temperature.[15]

For O preimplanted samples, a large number of vacancies as well as O atoms are produced during O implantation. H ions favorably interact with these vacancy defects during subsequent H implantation, leading to the formation of H-vacancy complexes. By absorbing more gas atoms and vacancies, the H-vacancy complexes grow bigger and bigger in the annealing process and eventually become the cavities that can be observed by XTEM (see Fig. 1). It is reported that the creation and thermal growth of cavities are mainly achieved by exchanging both gas atoms and the implantation induced vacancy defects.[2,16] Therefore, the formation of cavities under sequential implantation of O and H ions is mainly attributed to the large number of vacancy defects generated by O preimplantation. For a cavity, O[17,18] and H[12–14] atoms can be trapped on the cavity walls by chemisorption. The faceted cavities shown in Fig. 1b may be caused by uneven chemisorption of gas atoms between the cavity walls. The ratio of trapped gas atoms between different cavity walls could be equal to the area ratio. Unfortunately, we cannot obtain the area of a cavity wall from XTEM images. For a larger cavity, a large amount of atoms are trapped on the cavity walls. The difference in the number of trapped atoms between each cavity wall is small, especially compared with the total trapped atoms. Thus, the larger cavities usually have an almost elliptic shape, as shown in Fig. 1c.

For H preimplanted samples, H atoms as well as H-related defects are produced during H implantation. But O ions are much bigger than H ions. During post O implantation, O atoms physically collide with the existing H-related defects and destroy the structures of these defects, leaving a large density of dangling bonds. Previous studies have shown that He post-implantation at higher energy can destroy the structures induced by H preimplantation at lower energy.[19] The active H atoms will react with the dangling bonds and promote the formation of platelets in the annealing process, as described above. Consequently, the formation of platelets under sequential

implantation of H and O ions is caused by damage on the structures of H-related defects by the heavier O post-implantation.

It should be mentioned that the depth of the defect band in the two samples is deeper than the projected range of H and O ions. According to Nguyen's study, the presence of a noncontinuous amorphous zone induced by co-implantation of H and He ions in a higher total dose pushes H-platelet formation and fractures deeper into the Si lattice.[20] Although no amorphous zone is found in our XTEM images, the presence of large strain and highly damaged zone can also lead to a deeper defect band. Nevertheless, in order to clarify the reasons for a deeper defect band, more experiments should be subsequently carried out.

H and O implantation into Si generates a large amount of vacancy-type defects. Positrons are sensitive to the detection of vacancy-type defects by the phenomenon of positron trapping, which occurs in open-volume regions of any kind of crystalline material. Therefore, SPAS is used to study the thermal evolution of vacancy-type defects in Si under different implantation sequences. The mean depth z (nm) of the incident positrons is given by $z = (A/\rho)E^n$, where E (keV) is the incident positron energy and ρ (g cm^{-3}) is the mass density of the target. For a Si target, the constants A and n are empirically determined to be 4.0 (μg cm^{-2} keV^{-n}) and 1.6, respectively. Figure 4 shows the SPAS results of O preimplanted samples. The parameter S is low at the sample surface, owing to the positrons back diffusion to the surface. In the vicinity of the sample surface ($E \approx 4$ keV and $z \approx 160$ nm), the damage produced by H and O implantation is small, such as monovacancy, divacancy, and a few vacancy clusters. The majority of the vacancy-type defects are divacancies, which are easy to be dissolved in the annealing temperature range of 200°C to 300°C.[21] With increasing the annealing temperature, the vacancies get further dissolution. Thus, the decrease of parameter S with increasing the temperature at the near-surface is related to the dissolution of small vacancy-type defects. Nuclear scatterings occur for the implants and the Si target around the projected ranges of H and O ions (E is 6 keV–9 keV and z is 300 nm–580 nm). The size of defects increases from vacancy clusters into larger micro-voids and H/O related complexes. It is worth noting that once the H/O atoms penetrate into the vacancy type defects, these defects cannot be recognized by positrons. The decrease of parameter S at 300°C for annealing is related to the dissolution of small open-volume vacancy-type defects such as divacancies. With increasing the annealing temperature to 450°C, the micro-voids and complexes at the projected range grow thermally by absorption of vacancies and H/O atoms. Eventually, the large cavities are observed by XTEM measurements, as shown in Fig. 1. However, these complexes cannot be recognized by positrons because of the presence of H/O atoms, leading to a further decrease of S.

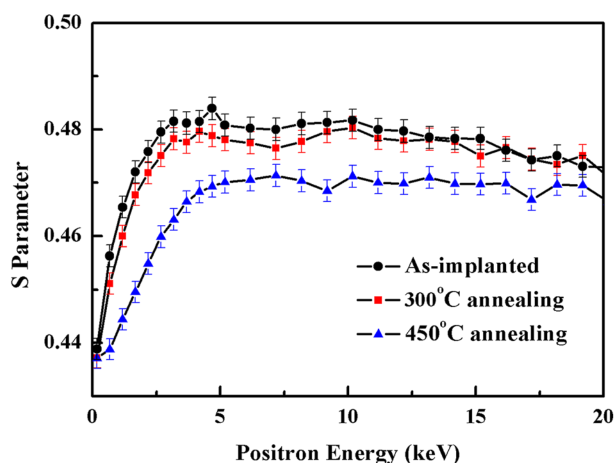

Fig. 4. SPAS measurements showing the S parameter as a function of positron incident energy in Si samples by sequential implantation of 190 keV O and 40 keV H ions and followed by annealing at different temperatures.

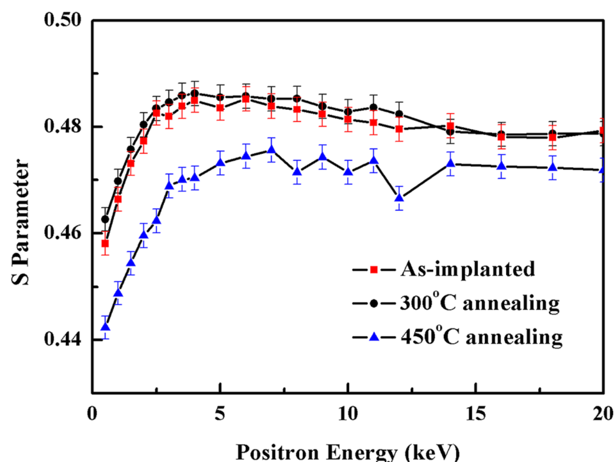

Fig. 5. SPAS measurements showing the S parameter as a function of positron incident energy in Si samples by sequential implantation of 40 keV H and 190 keV O ions and followed by annealing at different temperatures.

The SPAS results of H preimplanted sample are shown in Fig. 5. Comparing Figs. 4 and 5, S changes in the same way. With increasing annealing temperature, the parameter S decreases monotonically. However, the parameters S of H preimplanted samples are a little higher than O preimplanted samples. For H preimplanted samples, H implantation produces a number of H-related complexes, whose structure is, however, destroyed by the subsequent O implantation. Some vacancies are released to capture positrons, leading to the higher S in as-implanted samples. After annealing at 450°C, the parameters S in the near surface are almost the same for the two kinds of samples. Around the projected ranges of H and O ions, the parameter S is higher in H

preimplanted samples. This is due to the poor thermal stability of small defects. During annealing, they can be decomposed into gas atoms and vacancies. XTEM results also confirm that the size of platelets is smaller than that of the cavities. Although XTEM samples are annealed at 800°C, the defect morphologies can be considered as the reflection of the thermal evolution of implanted defects.

CONCLUSIONS

The defects formation and thermal evolution in H and O co-implanted Si samples have been characterized. We show that the defect morphology depends strongly on the implantation sequence of H and O ions. Large bubbles are observed in O preimplanted samples, which are attributed to the large number of vacancies produced by O and H implantation in promoting the thermal evolution of H-related complexes. However, small platelets in a high density appear in H preimplanted samples. This is mainly because the subsequent heavier O implantation destroys the structure of H-related complexes as well as micro-voids.

ACKNOWLEDGEMENTS

This work is supported by National Natural Science Foundation of China (No. 11275138), Tianjin Application Fundamental and Frontier Technology Research Project (No. 14JCYBJC17100 and No. 15JCYBJC16700) and Scientific Research Foundation of Tianjin University of Technology and Education (No. KYQD11001).

REFERENCES

1. M. Bruel, *Electron. Lett.* 31, 1201 (1995).
2. G.F. Cerofolini, F. Corni, S. Frabboni, C. Nobili, G. Ottaviani, and R. Tonini, *Mater. Sci. Eng. R* 27, 1 (2000).
3. T. Höchbauer, A. Misra, M. Nastasi, and J.W. Mayer, *J. Appl. Phys.* 92, 2335 (2002).
4. Q.Y. Tong, T.H. Lee, P. Werner, U. Gösele, R.B. Bergmann, and J.H. Werner, *J. Electrochem. Soc.* 144, L111 (1997).
5. Q.Y. Tong, Y.L. Chao, L.J. Huang, and U.M. Gösele, *Electron. Lett.* 35, 341 (1999).
6. I. Radu, I. Szafraniak, R. Scholz, M. Alexe, and U. Gösele, *J. Appl. Phys.* 94, 7820 (2003).
7. A. Agarwal, T.E. Haynes, V.C. Venezia, O.W. Holland, and D.J. Eaglesham, *Appl. Phys. Lett.* 72, 1086 (1998).
8. Z. Wang, J. Wang, and C.L. Liu, *Nucl. Instr. Methods B* 339, 58 (2014).
9. J.F. Ziegler and J.P. Biersack, SRIM (stopping and range of ions in matter) computer code (2012). http://www.srim.org. Accessed 15 Oct 2012.
10. S.J. Pearton, J.W. Corbett, and M. Stavola, *Hydrogen Incorporation in Crystalline Semiconductors* (Berlin: Springer, 1992), pp. 4–27.
11. M.K. Weldon, V.E. Marsico, Y.J. Chabal, A. Agarwal, D.J. Eaglesham, and J. Sapjeta, *J. Vaccum Sci. Technol. B* 15, 1065 (1997).
12. J.K. Lee, M. Nastasi, N.D. Theodore, A. Smalley, T.L. Alford, J.W. Mayer, M. Cai, and S.S. Lau, *J. Appl. Phys.* 96, 280 (2004).
13. P. Nguyen, K.K. Bourdelle, T. Maurice, N. Sousbie, A. Boussagol, X. Hebras, L. Portigliatti, F. Letertre, A. Tauzin, and N. Rochat, *J. Appl. Phys.* 101, 033506 (2007).
14. N. Desrosiers, A. Giguere, O. Moutanabbir, and B. Terreault, *Appl. Phys. Lett.* 87, 231908 (2005).
15. P. Gaworzewski and K. Schmalz, *Phys. Status Solidi A* 58, K223 (1980).
16. V. Raineri, M. Saggio, and E. Rimini, *J. Mater. Res.* 15, 1449 (2000).
17. D.M. Follstaedt, S.M. Myers, G.A. Petersen, and J.W. Medernach, *J. Electron. Mater.* 25, 157 (1996).
18. J.H. Evans, A. Van Veen, and C.C. Griffioen, *Nucl. Instr. Methods B* 28, 360 (1987).
19. O. Moutanabbir and B. Terreault, *Appl. Phys. Lett.* 86, 051906 (2005).
20. P. Nguyen, I. Cayrefourcq, K.K. Bourdelle, A. Boussagol, E. Guiot, N.B. Mohamed, N. Sousbie, and T. Akatsu, *J. Appl. Phys.* 97, 083527 (2005).
21. J. Keinonen, M. Hautala, E. Rauhala, V. Karttunen, A. Kuronen, J. Räisänen, J. Lahtinen, A. Vehanen, E. Punkka, and P. Hautojärvi, *Phys. Rev. B* 37, 8269 (1988).